Publishing Excellence
Inspiring Progress
ARISTON PUBLICATIONS
ChemSci Advances
ISSN: 2997-9587 www.aristonpubs.com/chemsci-advances https://doi.org/10.69626/csa.2025.0114

RESEARCH ARTICLE

pH–Controlled Synthesis of Magnetic Fe_3O_4 Nanoparticles for Enhanced Crystal Violet Dye Degradation via Photo–Fenton Process

Ankita Patil [1], Rupali Chavan [1], Aishwarya Jadhav [2], Aviraj Jatratkar [2], Rahul Patil [2], Nilesh Pawar [3], Ashok Chougale [1,*]

ABSTRACT: The increasing industrialization has exacerbated the scarcity of clean water, making wastewater treatment and dye degradation critical environmental challenges. Magnetic nanoparticles (MNPs) have emerged as promising catalysts for efficient wastewater remediation due to their high surface area, magnetic recoverability, and catalytic activity. This study investigates the influence of synthesis pH (6–9) on the structural, morphological, and catalytic properties of Fe_3O_4 MNPs synthesized via the co-precipitation method. Comprehensive characterization using XRD, FTIR, SEM, and EDX confirmed the formation of cubic crystalline Fe_3O_4 with phase purity, where pH variations significantly influenced particle size, morphology, and surface charge. SEM analysis revealed that pH 7 yielded well-dispersed nanoparticles with optimal porosity, while extreme pH conditions (6, 8, 9) led to irregular aggregation. The catalytic efficiency of the synthesized MNPs was evaluated in the photo-Fenton degradation of crystal violet (CV) dye under visible light. The MNPs synthesized at pH 7 exhibited superior performance, achieving 94% CV degradation within 60 min, compared to 88–89% degradation at other pH values (requiring 75–150 min). Further parametric studies established optimal conditions: 0.1 mM CV, 100 mg/L catalyst dosage, 0.1 M H_2O_2, and neutral pH. The catalyst demonstrated excellent reusability, retaining 82% efficiency after five consecutive cycles. These findings highlight the critical role of synthesis pH in tailoring MNP properties for enhanced dye degradation, offering a sustainable and magnetically separable solution for industrial wastewater treatment.

Keywords: Magnetic nanoparticles (MNPs), pH-dependent synthesis, Crystal violet degradation, Photo-Fenton process, Fe_3O_4 nanoparticles, Wastewater treatment

Received: 29 August 2024; Revised: 27 October 2024; Accepted: 02 January 2025; Published Online: 03 February 2025

1. INTRODUCTION

In order to support life on Earth, water is necessary. However, for safe consumption, it must be devoid of dangerous chemicals and microbes [1,2]. Water resources are contaminated by various industrial activities worldwide [3]. Along with the industrial chemical products, some other commonplace items like insecticides, coatings, printing inks, adhesives, cleaning supplies, and personal care items, are the major causes of water pollution and now pose the biggest threat to water resources. The expanding textile, paper, and printing industries also pose a greater risk of water pollution due to their dyes and effluents containing hazardous elements [4]. The aforementioned industries particularly contain carcinogenic compounds such as dyes, the degradation of CV is the foucus of this study. Such a hazardous and carcinogenic compound harms society, and the ecosystem.

Hence, to address this widely recognised problem, scientists have looked into a number of practical ways to reduce or break down dyes [5]. Among synthetic dyes, the cationic dye crystal violet (CV) can create severe health and environmental issues, including cancer, eye irritation, and

[1] Department of Chemistry, The New College Kolhapur, Shivaji University Kolhapur, 416012, India.
[2] Department of Physics, Shri. Yashwantrao Patil Science College Solankur, Shivaji University Kolhapur, 416211, India.
[3] Department of Botany, The New College Kolhapur, Shivaji University, Kolhapur, India.

*Author to whom correspondence should be addressed:
ashokdchougale@gmail.com (Ashok Chougale)

water colouration [6]. Traditionally, numerous methods including adsorption, absorption, filtration, bio-sorption, biodegradation, ozonation, etc. were used to eliminate hazardous dye impurities from water supplies. These conventional treatment methods are inefficient, non-destructive and they transfer contaminants from one area of the water to another, resulting in secondary pollution [7][8]. To tackle this problem advanced oxidation processes such as Fenton, photocatalysis, and photo-Fenton were employed. Among these, the photo-Fenton reaction is straightforward, effective, and has a high reaction rate; the rate of this reaction can be increased by using nanoparticles as a catalyst, and it is a widely recognized and noteworthy topic. In the photo-Fenton process, simultaneous exposure to light can significantly accelerate the rate of dye degradation [9].

As mentioned earlier, the catalyst impacts the efficacy of the dye degradation reaction. Thus the preparation of the catalyst serves as a key factor. Therefore nowadays reasearcher are using the relatively new field of nanotechnology to prepare catalysts. Since nanostructured materials have superior surface properties such as high reactivity, increased surface area, and enhanced charge separation capacity; they may therefore show great promise for the application of electrical, optoelectronic, magnetic storage, biocatalysis, environmental remediation, and biomedical applications, catalysis is greatly aided by nanoscale magnetic structures [10-12]. Previously, researchers have reported dye degradation activity using traditional non-magnetic catalysts [13].

Non-magnetic nanoparticles are incapable of being influenced by magnetic fields whereas magnetic nanoparticles can be controlled and directed using external magnetic field. For the simple recovery of the magnetic nanoparticles, an external magnetic arena was used. Additionally, MNPs indicate the low solubility and reusability of the catalyst, which makes them more desirable for wastewater treatment. A thorough literature review of the dye degradation activity by the Fe_3O_4 MNP has great respond towards dye degradation [13]. The synthesis of magnetic nanoparticles using a chemical approach includes techniques such as electrolysis, pyrolysis, sol gel, solvothermal synthesis, chemical reduction of metal salts, phytochemical irradiation, and co-precipitation. Among this, co-precipitation is an simple and cheap method; therefore it was widey used for the synthesis of the nanoparticles. Lin et al has synthesized Fe_3O_4 nanoparticles using a co-precipitation technique on a rotating packed bed (RPB) in continuous mode. The size of Fe_3O_4 nanoparticles was also studied in terms of rotation speed, reactant and precipitant flow rates, and concentrations for Rhodamine B degradation. Experimental results reveal that a faster rotating speed and bigger flow rates of the reactants and precipitant are related with a lower size of Fe_3O_4 nanoparticles [14]. Sirivat et al synthesized Magnetite (Fe_3O_4) nanoparticles in his study via chemical co-precipitation. The architectures, shape, electrical conductivity, and magnetic properties of synthesized Fe_3O_4-NPs and gelatin coated- Fe_3O_4. NPs (GFe_3O_4 NPs) with and without drug loading (Mer-GFe_3O_4 NPs) were examined for pH values ranging from 8 to 12 during synthesis. The pH value was shown to alter particle size and shape, both of which were related to electrical and magnetic properties. The superparamagnetic behavior of synthesized Fe_3O_4 NPs is critical for biomedical applications because it prevents particle aggregation and enables the particles to re-disperse rapidly after the removal of magnetic field [15].

Kerroum et al. demonstrated co-precipitation approach for the manufacture of zinc ferrite ($ZnFe_2O_4$) MNPs. The pH range (9–12) influences structural, magnetic, and hyperthermia properties. As pH rises, size grows (19-33 nm) and form structural changes (polyhedral to spherical). Aggregation causes 19 nm MNPs to have higher coercive field and blocking temperature values [16]. Gnanaprakash et al. [6] studied that average particle size increases with initial pH 6.4 nm (pH 0.7), 7.6 nm (pH 1.5), and 9.9 nm (pH 3 and 4.7). Initial pH, temperature, and ultimate pH influence magnetite and goethite nanoparticle production. By regulating pH and temperature, the co-precipitation approach may produce pure magnetite nanoparticles free of goethite impurities [6]. From the above review literature is it clearly seen that pH-based variation during the synthesis of MNPs play important role in their activity.

In the current study, variation of the pH during synthesis of Fe_3O_4 MNPs were performed and their catalytic activity was evaluated. This Synthesized samples were examined by various characterisation techniques such as XRD, FTIR, SEM, and EDX. Among this characterisation, SEM analysis profoundly revealed that the variation of the pH during synthesis affects the surface morphology of the MNPs. While the shape and surface morphology of the catalyst plays a critical role during dye degradation reaction. Further, the effect of different operational parameters such as the concentration of CV, MNPs dosage, H_2O_2 dosage and initial pH of the solution was also evaluated. Morever, the reuse cycles were performed to test the reuse ability and stability of the MNPs.

2. EXPERIMENTAL DETAILS

2.1. Synthesis of Fe_3O_4 Magnetic Nanoparticles

Fe_3O_4 MNPs were synthesized via the co-precipitation method using ferric nitrate ($Fe(NO_3)_3 \cdot 9H_2O$) and glucose as precursors. Initially, 0.1 M aqueous solutions of ferric nitrate and glucose were prepared separately and mixed under vigorous stirring at 80°C to ensure homogeneity. The pH of the reaction mixture was carefully adjusted to 6, 7, 8, and 9 using dropwise addition of 0.1 M NaOH. The solution was continuously stirred for 1 h to facilitate complete precipitation. The resulting black precipitate was collected via magnetic separation, washed repeatedly with deionized water and ethanol to remove impurities, and then dried at 80°C for 12 h. The dried powder was calcined at 400°C for 2 h in a muffle furnace to enhance crystallinity and phase purity. The final product was stored in an airtight container for further characterization and catalytic studies. Figure 1(a)

shows the homogeneous dispersion of as-synthesized Fe_3O_4 magnetic nanoparticles (MNPs) in aqueous solution, while Figure 1(b) demonstrates their immediate magnetic response and rapid separation when an external magnetic field is applied, confirming their superparamagnetic properties and suitability for recyclable applications

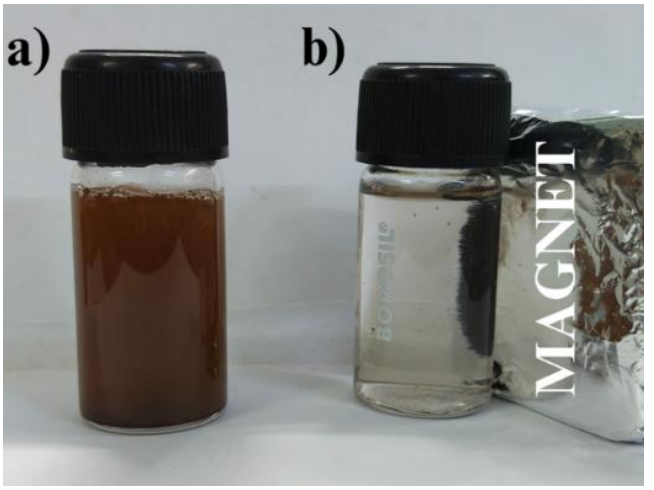

Fig. 1. (a) Aqueous suspension of as-synthesized Fe_3O_4 MNPs showing colloidal stability; (b) Magnetic separation of MNPs under an external magnetic field, demonstrating their superparamagnetic behavior.

2.2. Characterization Techniques

The structural and morphological properties of the synthesized MNPs were analyzed using multiple techniques. X-ray diffraction (XRD, Rigaku SmartLab) with Cu-Kα radiation (λ = 1.5406 Å) was employed to determine crystallinity and phase purity, with scans recorded in the 2θ range of 10–80°. Fourier-transform infrared spectroscopy (FTIR, PerkinElmer Spectrum Two) was performed in the range of 400–4000 cm^{-1} to identify functional groups and chemical bonding. Scanning electron microscopy (SEM, JEOL JSM-IT800) coupled with energy-dispersive X-ray spectroscopy (EDX) was used to examine surface morphology and elemental composition. Magnetic properties were assessed using a vibrating sample magnetometer (VSM), and UV-Vis spectroscopy (Evolution 201) monitored dye degradation kinetics.

2.3. Photo-Fenton Degradation Experiments:

The catalytic performance of the MNPs was evaluated in the degradation of crystal violet (CV) dye under visible light irradiation. A 0.1 mM CV solution was prepared, and 100 mg/L of MNPs (optimal dosage) was dispersed in the dye solution under constant stirring. Hydrogen peroxide (H_2O_2, 0.1 M) was added as an oxidant, and the reaction mixture was exposed to a 300 W halogen lamp (λ > 420 nm) to initiate the photo-Fenton process. Aliquots were collected at regular intervals, centrifuged to remove catalyst particles, and analyzed via UV-Vis spectroscopy at λ_{max} = 590 nm to determine residual dye concentration. Control experiments were conducted to assess the individual effects of H_2O_2, MNPs, and light irradiation. The degradation efficiency was calculated using the formula:

$$\text{Degradation } (\%) = \left(1 - \frac{C_t}{C_o}\right) \text{ X } 100$$

where C_0 and Ct represent initial and time-dependent dye concentrations, respectively.

2.4. Reusability Study

The stability and reusability of the MNPs were tested over five consecutive cycles. After each run, the catalyst was magnetically separated, washed with ethanol and water, dried at 80°C, and reused under identical conditions. The degradation efficiency was monitored to evaluate catalytic consistency.

3. RESULTS AND DISCUSSION

3.1. Characterization

3.1.1. X-ray Diffraction (XRD) Analysis

The crystalline structure and phase purity of the synthesized Fe_3O_4 magnetic nanoparticles (MNPs) at varying pH conditions (pH=6–9) were systematically investigated using X-ray diffraction (XRD). As shown in Figure 2, all samples exhibited characteristic diffraction peaks at 2θ = 30.4° (311), 35.8° (220), 43.8° (400), 54.4° (511), and 63.2° (440), which are in excellent agreement with the standard cubic spinel structure of magnetite (JCPDS card no. 00-001-1053) [4, 6]. The absence of secondary peaks (e.g., hematite or maghemite) confirms the phase purity of the synthesized MNPs. Notably, the (311) peak at 35.8° demonstrated the highest intensity across all samples, indicating preferential growth along this crystallographic plane. The sharp and well-defined peaks suggest high crystallinity, while the consistent peak positions across pH variants confirm that the cubic spinel structure is maintained regardless of synthesis pH. However, subtle variations in peak broadening were observed, with pH 7 showing the narrowest peaks, suggesting larger crystallite sizes at this condition. The crystallite size, calculated using the Debye-Scherrer equation, ranged between 12–18 nm, with pH 7 yielding the largest crystallites. This observation correlates with the enhanced catalytic activity of pH 7 MNPs, as larger crystallites typically exhibit fewer grain boundaries and improved charge carrier mobility. The XRD results collectively validate the successful synthesis of phase-pure Fe_3O_4 with pH-dependent crystallinity, where pH 7 optimized both structural order and crystallite size.

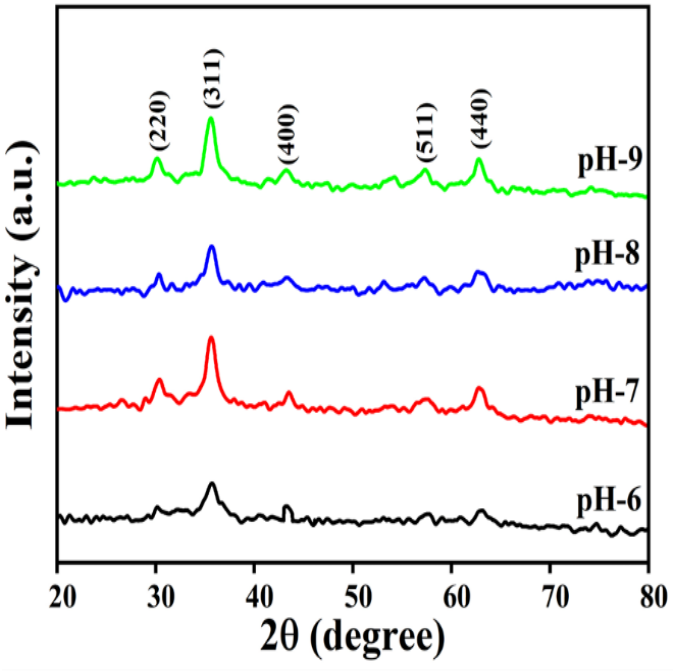

Fig. 2. XRD patterns of Fe_3O_4 MNPs synthesized at pH=6–9, confirming cubic spinel structure (JCPDS 01-1053) with indexed crystallographic planes.

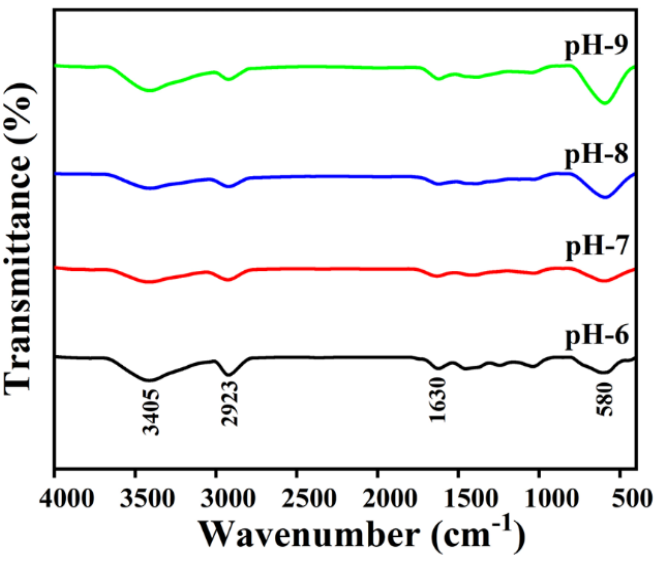

Fig. 3. FTIR spectra of pH-varied Fe_3O_4 MNPs showing Fe-O vibrations (~580 cm^{-1}) and surface hydroxyl groups (3405 cm^{-1}).

3.1.2. Fourier-Transform Infrared (FTIR) Spectroscopy

The chemical bonding and surface functionalization of the MNPs were analyzed using FTIR spectroscopy (Figure 3). All samples exhibited a dominant absorption band at ~580 cm^{-1}, attributed to the Fe–O stretching vibrations of the tetrahedral (Fe^{3+}) and octahedral (Fe^{2+}/Fe^{3+}) sites in the spinel lattice, confirming the formation of magnetite (Fe_3O_4). The band's position and intensity remained consistent across pH variants, indicating stable Fe–O bonding irrespective of synthesis conditions. A broad absorption band at 3405 cm^{-1} and a sharper peak at 1630 cm^{-1} were assigned to the O–H stretching and bending vibrations of adsorbed water molecules, respectively. These features arise from surface hydroxylation due to the aqueous synthesis environment, where exposed Fe and O atoms interact with water to form –OH groups. The intensity of these bands varied slightly with pH, with pH 7 showing the lowest –OH absorption, suggesting reduced surface hydration and potentially higher catalytic site availability. Additionally, a weak band at 2923 cm^{-1}, corresponding to C–H stretching vibrations, was observed in all samples, likely originating from residual glucose used in the synthesis. The absence of peaks above 2000 cm^{-1} (e.g., C=O or C≡N) rules out significant organic contamination [17, 18]. Notably, no shifts in Fe–O band positions were detected across pH variants, implying that pH primarily influences surface chemistry rather than bulk crystal chemistry [19, 20]. The FTIR data thus corroborate the XRD findings, confirming the formation of pure Fe_3O_4 with pH-modulated surface hydroxylation, which critically impacts catalytic activity.

3.1.3. Scanning Electron Microscopy (SEM) Analysis

SEM observations were utilised to determine the morphological parameters of the MNPs. Figure 4 reveals the strong correlation between the pH and surface morphology. The morphology of the MNPs at pH 6 (Figure 4 (a)) is seen to have irregular aggregation and a high degree of porosity. This moght be due to the pH being considerably lower than the point of zero charge (PZC) of Fe_3O_4, which is typically around pH 7.9. At this pH, the nanoparticles become more positively charged due to the protonation of surface hydroxyl groups, which strengthens electrostatic attraction and induces uncontrolled aggregation, resulting in larger, less-defined structures. As shown in Figure 4(b), the MNPs at pH 7 have a more structured and smooth morphology, because this pH is close to the PZC of Fe_3O_4, leading to minimal surface charge and weaker electrostatic interactions. As a result, the particles experience less aggregation and better dispersion in the solution, forming well-structured, monodisperse nanoparticles, while the higher surface area and pore volume at this pH may further enhance catalytic activity. The surface morphology become more porous and aggregated as we move towards the pH 8 (Figure 4(c)). As Fe_3O_4 undergoes deprotonation, its surface charge becomes more negative, enhancing electrostatic repulsion; however, an excess of hydroxyl ions can trigger uncontrolled nucleation, leading to loosely packed, porous structures that reduce nanoparticle stability and uniformity. Further, moving toward the pH 9 (Figure 4(d)) reveals irregular morphology with noteworthy aggregation. At pH 9, dispersion was enhanced due to increased negative surface charge, while highly alkaline pH triggered rapid nucleation and iron hydroxide precipitation, forming poorly defined, loosely packed clusters that reduce surface area and may impact catalytic efficiency.

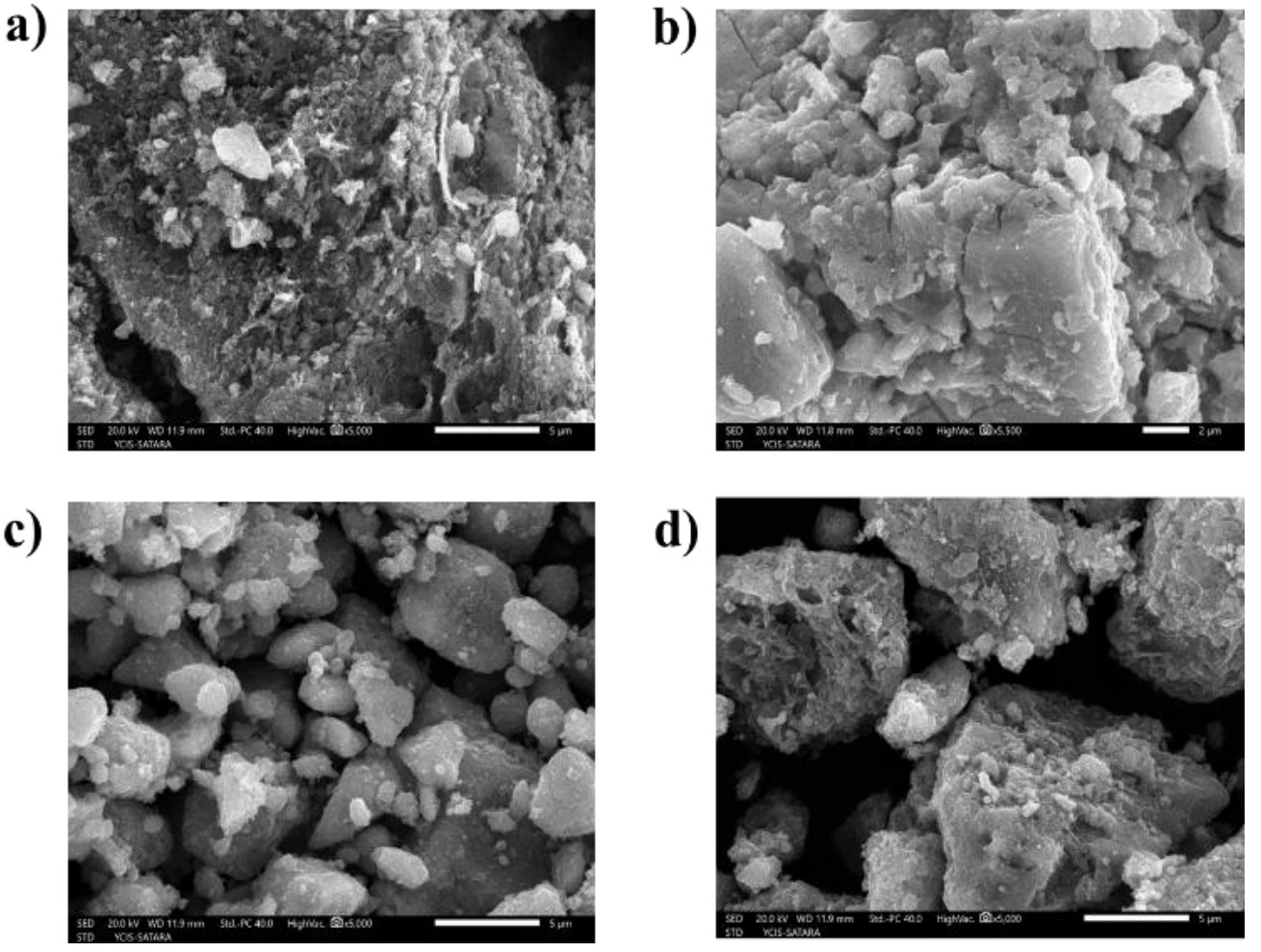

Fig. 4. SEM images of Fe_3O_4 MNPs synthesized at (a) pH 6, (b) pH 7, (c) pH 8, and (d) pH 9, revealing morphology dependence on synthesis pH.

3.1.4. Energy Dispersive X-ray (EDX) Spectroscopy Analysis

The elemental composition and chemical purity of the synthesized Fe_3O_4 nanoparticles were rigorously characterized using Energy Dispersive X-ray (EDX) spectroscopy, as presented in Figure 5 (a-d). The EDX spectra of all pH variants (pH=6-9) exhibited prominent emission peaks at 0.5 keV (O Kα), 6.1 keV (Fe Kα), and 7.0 keV (Fe Kβ), confirming the presence of iron and oxygen as primary constituents. The additional peak observed at 0.9 keV corresponds to Fe Lα transitions, while the consistent detection of carbon signals (~0.28 keV) across all samples originates from residual glucose used in the synthesis process. Quantitative EDX analysis revealed an average atomic composition of 43.93% oxygen, 20.12% iron, and 35.95% carbon, with the elevated carbon content (35.95%) attributed to both organic precursors and potential surface adsorption during sample preparation [21]. Notably, the Fe/O ratio remained stable across pH variations, indicating consistent stoichiometry of the magnetite phase (Fe_3O_4). The minor variations in elemental percentages (<2%) between samples suggest that synthesis pH primarily affects morphological rather than compositional properties. The absence of extraneous elemental peaks confirms the high purity of the synthesized nanoparticles, with no detectable impurities from synthesis reagents or equipment. These findings corroborate the XRD and FTIR results, collectively verifying the successful formation of phase-pure Fe_3O_4 nanoparticles with uniform elemental distribution regardless of synthesis pH conditions.

3.2. Dye Degradation by Photo-Fenton Process

The catalytic performance of pH-varied Fe_3O_4 MNPs was systematically evaluated through crystal violet (CV) degradation via the photo-Fenton process, as illustrated in Figure 6. A clear pH-dependence was observed in degradation efficiency, where MNPs synthesized at pH 7 demonstrated superior catalytic activity, achieving 94% CV degradation within just 60 minutes.

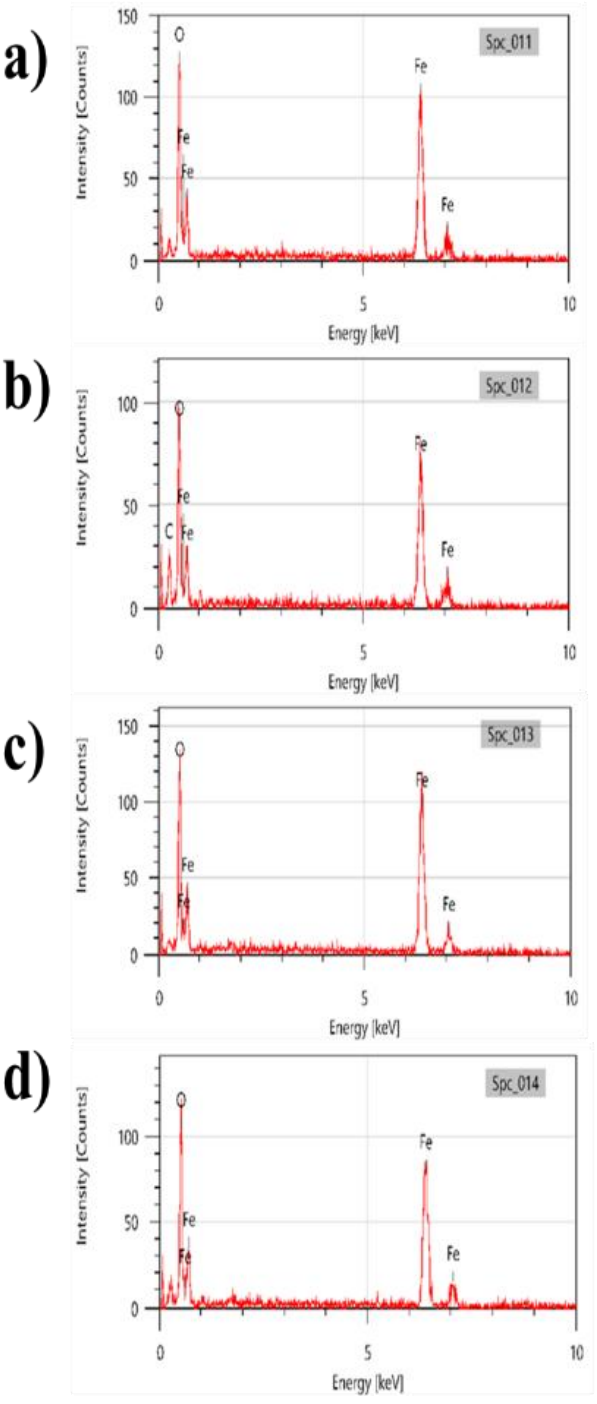

e) Elements	Mass (%)	Atom (%)
O	25.79±0.98	54.822±2.7
Fe	74..21±2.5	45.18±1.52
Total	100.00	100.00

f) Elements	Mass (%)	Atom (%)
C	19.12±0.88	35.95±1.66
O	31.13±1.33	43.93±1.87
Fe	49.75±2.06	20.12±0.83
Total	100.00	100.00

g) Elements	Mass (%)	Atom (%)
O	25.79±0.98	54.82±2.07
Fe	74.21±2.50	45.18±1.52
Total	100.00	100.00

h) Elements	Mass (%)	Atom (%)
O	27.24±1.08	56.65±2.26
Fe	72.76±2.71	43.35±1.61
Total	100.00	100.00

Fig. 5. (a–d) EDX spectra and (e–h) elemental composition tables of Fe_3O_4 MNPs at pH 6–9, confirming Fe/O atomic ratios and carbon residuals.

In contrast, nanoparticles prepared at pH 6, 8, and 9 required extended reaction times (75-150 minutes) to reach comparable degradation levels (88-89%). This enhanced performance of pH 7 MNPs directly correlates with their optimal structural characteristics observed in characterization studies - intense XRD peaks indicating high crystallinity, favorable surface morphology with increased pore volume from SEM analysis, and minimal surface hydroxylation from FTIR data. The degradation kinetics followed pseudo-first-order behavior, with pH 7 MNPs exhibiting the highest rate constant (0.045 min^{-1}), approximately 1.5-2 times greater than other pH variants.

Control experiments (Figure 7) provided critical mechanistic insights: (1) CV-only systems showed negligible degradation (13%), confirming dye stability under illumination; (2) CV+H_2O_2 systems achieved 38.1% degradation, demonstrating limited oxidative capacity without catalyst; (3) CV+Fe_3O_4 systems reached 53.7% degradation, revealing the nanoparticles' photocatalytic activity through electron-hole pair generation [22]; and (4)

the complete photo-Fenton system (CV+H_2O_2+Fe_3O_4) achieved 94% efficiency, highlighting the synergistic effect of iron-catalyzed hydroxyl radical (•OH) generation and photocatalytic activation [23]. The spectral evolution in complete systems showed progressive diminishment of CV's characteristic 590 nm absorbance band, accompanied by a hypsochromic shift, suggesting simultaneous N-demethylation and chromophore cleavage. These results establish that pH 7 optimized both the structural properties of MNPs and their interfacial charge transfer dynamics, enabling efficient H_2O_2 activation into •OH radicals while minimizing charge recombination - key factors governing the enhanced photo-Fenton activity observed.

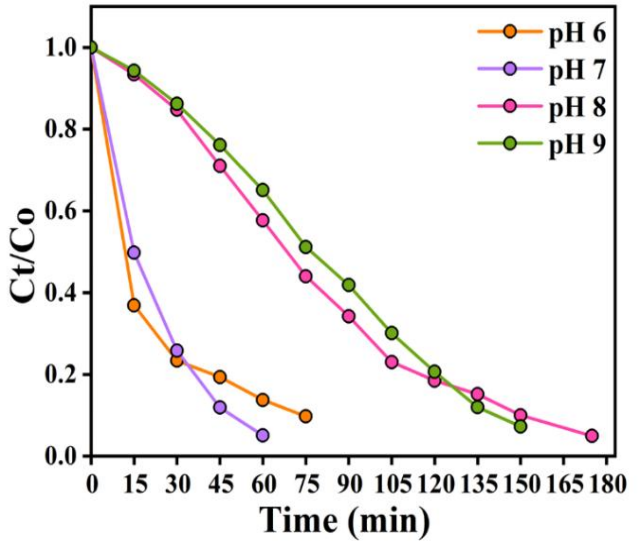

Fig. 6. Comparative photo-Fenton degradation efficiency of CV dye using Fe_3O_4 MNPs synthesized at different pH values (ph=6–9).

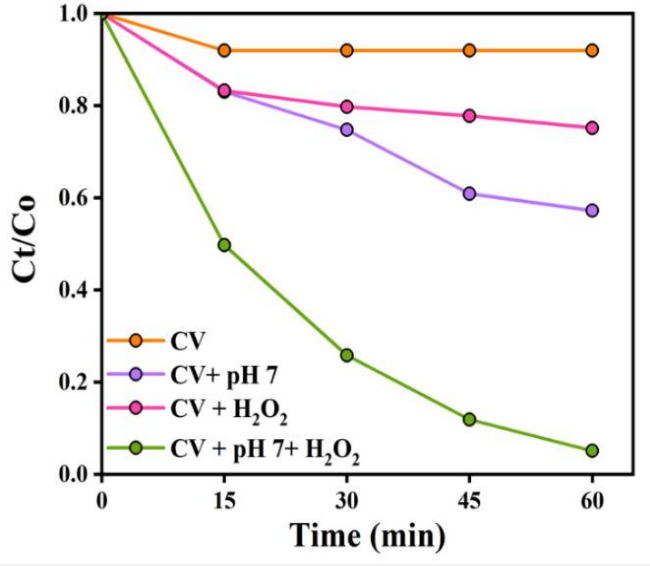

Fig. 7. Control experiments for CV degradation: (i) CV only, (ii) CV+H_2O_2, (iii) CV+MNPs, and (iv) complete photo-Fenton system (CV+H_2O_2+MNPs).

Figure 8 demonstrates a series of ultraviolet-visible (UV-Vis) absorption spectra collected at regular intervals during the catalytic degradation of crystal violet (CV) dye using iron oxide (Fe_3O_4) magnetic nanoparticles synthesized at pH 7. The spectra demonstrate the progressive decrease in intensity of the characteristic absorption peak at 590 nm, which corresponds to the chromophoric structure of the CV dye molecules. This systematic reduction in peak intensity directly correlates with the extent of dye degradation over time, providing quantitative evidence of the catalytic efficiency of the pH-7 Fe_3O_4 nanoparticles. The time-dependent spectral changes illustrate the breakdown of CV's conjugated π-electron system through oxidative cleavage, with complete diminishment of the 590 nm peak indicating near-total degradation of the dye molecules. The figure serves as direct spectroscopic proof of the photo-Fenton catalytic activity, showing how the nanoparticle catalyst facilitates the stepwise destruction of the dye's molecular structure under experimental conditions. The specific mention of pH-7 nanoparticles references earlier results showing these particles exhibit optimal catalytic performance compared to those synthesized at other pH values.

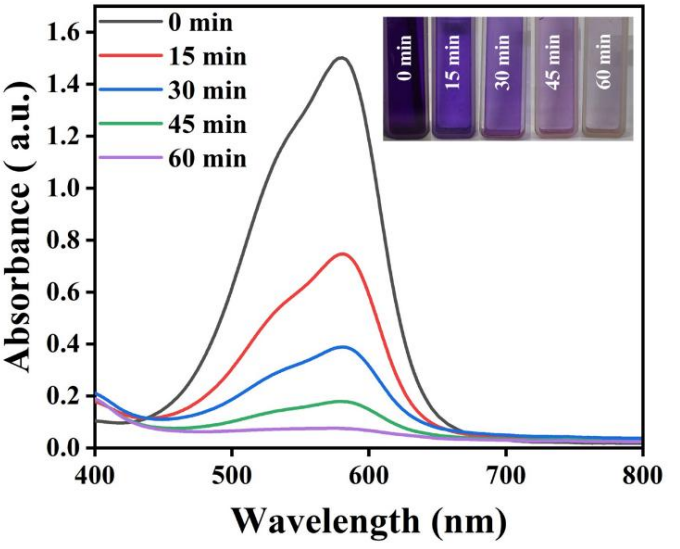

Fig. 8. Time-dependent UV-Vis absorbance spectra of CV degradation by pH-7 Fe_3O_4 MNPs, showing peak diminishment at 590 nm.

3.2.1. Effect of H_2O_2 Dosage on Dye Degradation

The concentration of hydrogen peroxide (H_2O_2) plays a critical role in the photo-Fenton degradation process, as it directly influences the generation of hydroxyl radicals (•OH), the primary reactive species responsible for dye degradation. Figure 9 demonstrates the impact of varying H_2O_2 concentrations (0.05–0.2 M) on the degradation efficiency of crystal violet (CV) using Fe_3O_4 MNPs synthesized at pH 7. A clear trend was observed: as the H_2O_2 concentration increased from 0.05 M to 0.1 M, the degradation efficiency significantly improved from 68% to 94%. This enhancement

is attributed to the increased availability of H_2O_2 molecules, which react with surface Fe^{2+}/Fe^{3+} sites on the MNPs to produce a greater quantity of •OH radicals through the Fenton ($Fe^{2+} + H_2O_2 \rightarrow Fe^{3+} + •OH + OH^-$) and photo-Fenton ($Fe^{3+} + H_2O_2 + h\nu \rightarrow Fe^{2+} + •OOH + H^+$) reactions.

However, further increasing the H_2O_2 concentration beyond 0.1 M (0.15–0.2 M) did not yield additional improvements in degradation efficiency. This plateau effect occurs due to two competing mechanisms: (1) At excessive H_2O_2 concentrations, the surplus H_2O_2 acts as a scavenger of •OH radicals, converting them into less reactive hydroperoxyl radicals (•OOH) via the reaction $H_2O_2 + •OH \rightarrow H_2O + •OOH$. (2) The formation of •OOH radicals (redox potential: 1.65 V) is less favorable for dye degradation compared to •OH radicals (redox potential: 2.8 V), leading to a decline in overall oxidative capacity. Additionally, high H_2O_2 concentrations may promote the recombination of •OH radicals or deactivate catalytic sites on the Fe_3O_4 surface through excessive Fe^{2+} oxidation to Fe^{3+}, which slows down the Fenton cycle.

The optimal H_2O_2 concentration of 0.1 M was therefore selected for subsequent experiments, as it provided the ideal balance between •OH radical generation and minimization of scavenging effects. This result highlights the importance of optimizing oxidant dosage in advanced oxidation processes to achieve maximum degradation efficiency while avoiding reagent overuse. The findings align with previous studies [13, 24, 25] and reinforce the need for precise control of H_2O_2 in photo-Fenton systems for wastewater treatment applications.

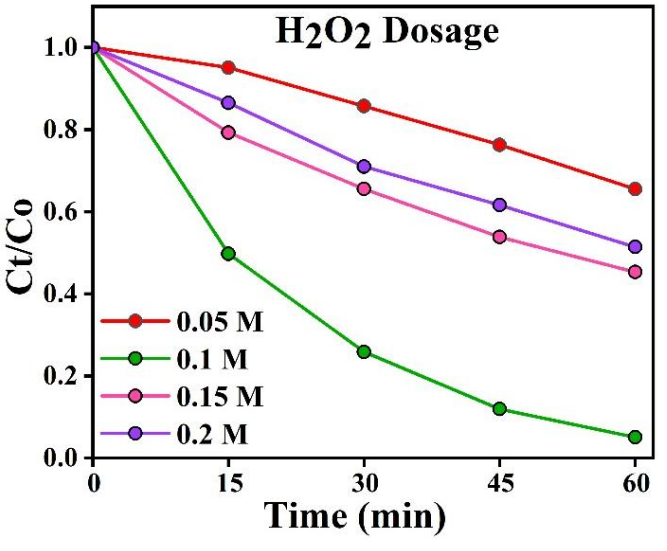

Fig. 9. Effect of H_2O_2 concentration (0.05–0.2 M) on CV degradation efficiency, with optimal performance at 0.1 M.

3.2.2. Effect of Initial pH on Dye Degradation

The surface-charge characteristics of the photo-Fenton reaction are influenced by the solution's initial pH. The surface charges of the catalysts, oxidants and pollutant species that are present in the reaction system are connected to the pH of the solution. Thus, the impact of pH changes from 3 to 9 on the removal of crystal violet (CV) was examined. As seen in Figure 10, experiments were conducted in the pH range of 3 to 9 to examine the impact of pH on CV degradation. These experiments were conducted with all other operating settings held constant. As illustrated in Figure 10, an increase in the percentage of dye degradation was observed as pH was raised from 3 to 9. At pH 3, 47% of CV degradation was observed; while 76% CV degradation was observed at pH 5. At neutral pH 7, 94% catalytic activity was enhanced by the catalysts. Lastly, pH 9 showed comparatively higher dye degradation. According to the observations, pH 7 is the ideal range for Fe_3O_4 to degrade CV [26, 27].

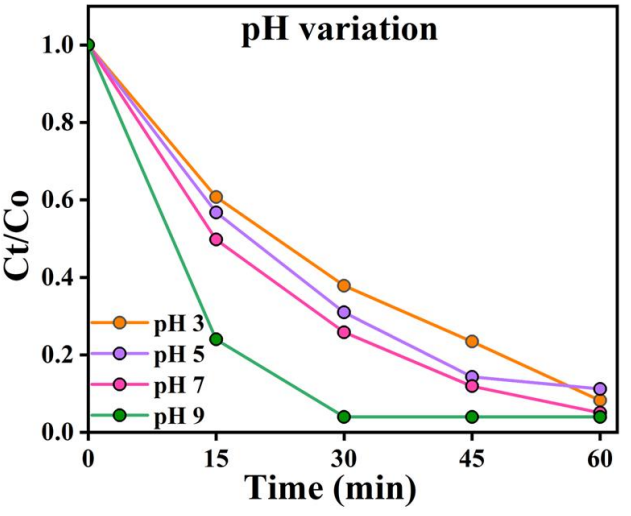

Fig. 10. pH-dependent CV degradation profiles (pH 3–9) demonstrating maximal efficiency at neutral pH (7).

3.2.3. Effect of Catalyst on Dye Degradation

Catalyst acts as a source of the activator causing H_2O_2 to produce ·OH. Therefore, the dosage of the catalyst has a major impact on the degradation efficiency. Figure 11 demonstrates how the catalyst dose affects the degradation activity. Since the higher catalyst dosage provide more active sites for the generation of ·OH radicals, increasing the catalytic efficiency. It can be concluded that the degradation accelerated as the amount of catalyst increased from 78 to 94% when the dosage was increased from 50 to 100 mg/L. However, when the catalyst dosage was raised from 150 to 200 mg/L, the degradation efficiency somehow dropped from 94 to 80%. This phenomenon can be explained by the possibility that a high concentration of catalyst in the solution may undergo the suspension more turbid and scatter light, which may decrease the system's ability to absorb the light. Another reason might be the quantity of accessible radicals which might be decreased by competing reactions brought on by the high catalyst dose ($Fe^{2+} + ·OH \rightarrow Fe^{3+} + OH^-$). The ideal catalyst concentration in this investigation

was 100 mg/L, as illustrated in Figure 11 [28, 29].

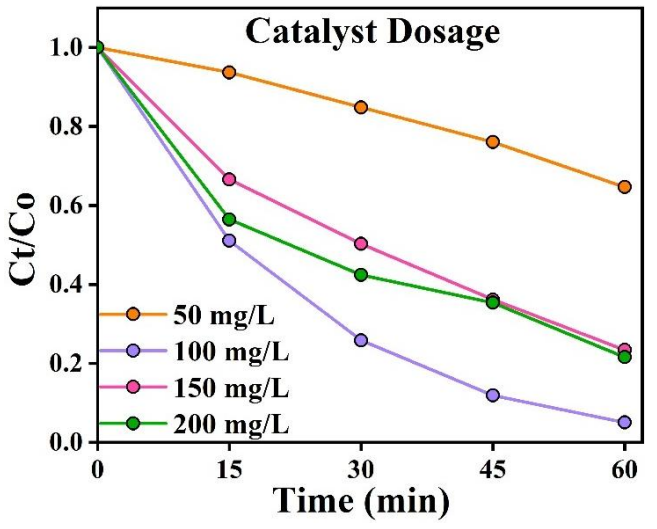

Fig. 11. Catalyst dosage effect (50–200 mg/L) on CV degradation, showing optimal performance at 100 mg/L Fe_3O_4 MNPs.

3.2.4. Effect of Initial Dye Concentration on Dye Degradation

The impact of dye doses on degradation rate is a crucial standpoint for its application purpose. To test photo-Fenton dye degradation, dye solutions with varying initial concentrations (0.05 to 0.2 mM) were prepared. The impact of initial CV concentration on the dye degradation processes is depicted in the Figure 12. It is seen that, above 90% of the CV was deteriorated by photo-Fenton processes at the starting dye concentration 0.05 and 0.1 mM. Due to easily accessible hydroxyl radicals, the dye is efficiently broken down at this dye concentrations. There is a drop in degradation efficacy for 0.15 to 0.2 mM. This scenario occurred with increased initial concentration; high contaminant load reduces the penetration of photons into the solution, which turns into the reduction of the generation of ·OH radicals. The limited catalytic active surface area was also reason behind this reduced degradation ability [30, 31]. Hence for effective degradation, the hydroxyl radical and dye molecules must be balanced.

3.2.5. Reuse

For industrial applications, the separation and consecutive use of catalyst plays a critical role. Thus photo-Fenton reaction was carried out five times with the same collected catalyst under the same operating conditions in order to assess the reusability of as synthesized MNPs. In Figure 13, the elimination profiles of CV for each of the five cycles are shown. In the first and second run, above 94% of CV was removed. Further, this degradation slowed down and removal efficiency dropped to 87, 85.5, 82% in the third, fourth, and fifth run. This result depicts that the degradation ability of the catalyst did not drop significantly even after its fifth reuse. Adsorbed CV molecules occupying Fe_3O_4 active sites may be the cause of the slight reduction in degradation efficiency during the reuse cycles. Additionally, the composite's corrosion in subsequent cycles may lessen the leaching of iron species from the material [32]. However, the adsorbed CV may be degraded and Fe_3O_4 surface reactivated in the middle stages of the process due to the presence of H_2O_2, which might have caused the degradation of CV to proceed at later stages. According to the findings observed, the catalyst can be used repeatedly and exhibits good stability [26, 33].

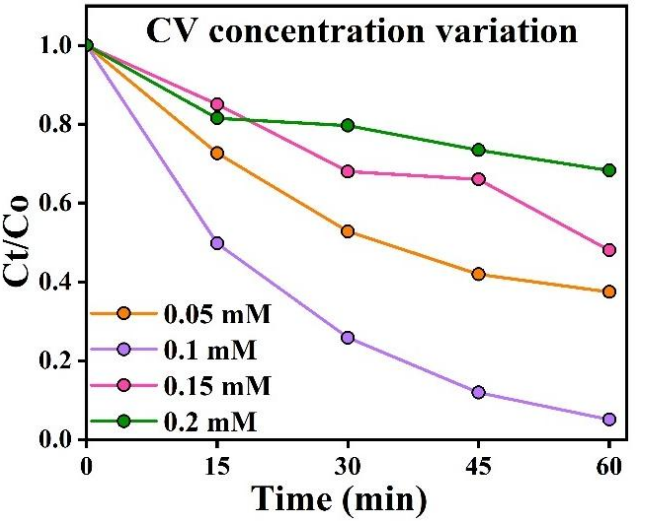

Fig. 12. Influence of initial CV concentration (0.05–0.2 mM) on degradation kinetics, highlighting reduced efficiency at higher concentrations.

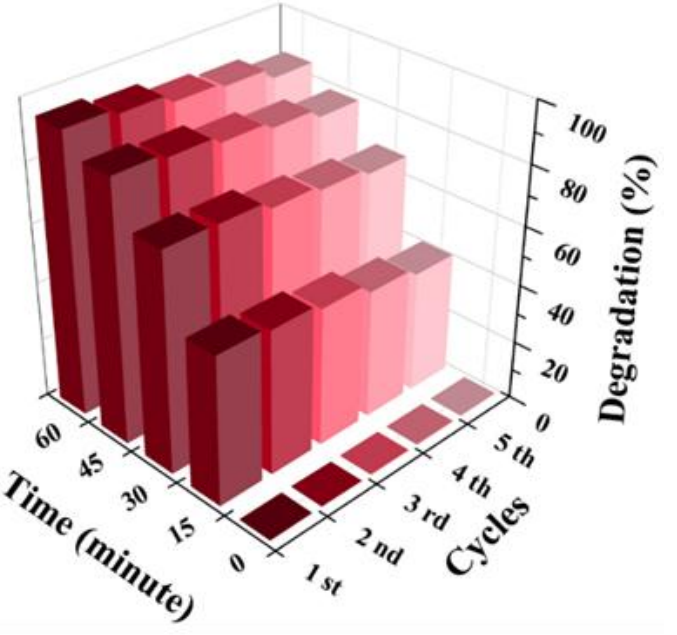

Fig. 13. Reusability test of Fe_3O_4 MNPs over 5 photo-Fenton cycles, demonstrating retained catalytic activity (>82%).

4. CONCLUSION

This study demonstrated the significant influence of synthesis pH on the structural and catalytic properties of Fe_3O_4 magnetic nanoparticles (MNPs) for efficient crystal violet (CV) dye degradation via the photo-Fenton process. The co-precipitation method facilitated the formation of cubic crystalline Fe_3O_4, with XRD and FTIR confirming phase purity and Fe-O bonding. SEM analysis revealed that pH 7 yielded uniformly dispersed nanoparticles with optimal porosity, whereas extreme pH conditions (6, 8, 9) resulted in irregular aggregation due to altered surface charge dynamics. The MNPs synthesized at pH 7 exhibited exceptional catalytic activity, achieving 94% CV degradation within 60 min under visible light, outperforming other pH variants (88–89% degradation in 75–150 min). Parametric optimization established 0.1 mM CV, 100 mg/L catalyst dosage, and 0.1 M H_2O_2 as ideal conditions, with neutral pH (7) proving most effective due to balanced hydroxyl radical generation and dye adsorption. The catalyst also demonstrated remarkable reusability, maintaining 82% efficiency after five cycles, attributed to its structural stability and magnetic recoverability. These findings underscore the critical role of synthesis pH in tailoring MNP morphology and surface properties for enhanced photocatalytic applications. The study presents Fe_3O_4 MNPs as a sustainable, cost-effective, and reusable solution for industrial wastewater treatment, addressing the pressing need for efficient dye removal technologies. Future work could explore hybrid nanocomposites and mechanistic studies to further improve degradation kinetics for complex industrial effluents.

DECLARATIONS

Ethical Approval

We affirm that this manuscript is an original work, has not been previously published, and is not currently under consideration for publication in any other journal or conference proceedings. All authors have reviewed and approved the manuscript, and the order of authorship has been mutually agreed upon.

Funding

Not applicable

Availability of data and material

All of the data obtained or analyzed during this study is included in the report that was submitted.

Conflicts of Interest

The authors declare that they have no financial or personal interests that could have influenced the research and findings presented in this paper. The authors alone are responsible for the content and writing of this article.

Authors' contributions

All authors contributed equally in the preparation of this manuscript.

REFERENCE

[1] A. Kalra and A. Gupta, 'Recent advances in decolourization of dyes using iron nanoparticles: A mini review', *Mater. Today Proc.*, vol. 36, no. xxxx, pp. 689–696, 2019, doi: 10.1016/j.matpr.2020.04.677.

[2] P. Xu *et al.*, 'Use of iron oxide nanomaterials in wastewater treatment: A review', *Sci. Total Environ.*, vol. 424, pp. 1–10, 2012, doi: 10.1016/j.scitotenv.2012.02.023.

[3] J. Singh, P. Yadav, A. K. Pal, and V. Mishra, 'Water Pollutants: Origin and Status', pp. 5–20, 2020, doi: 10.1007/978-981-15-0671-0_2.

[4] M. Chang and Y. hsin Shih, 'Synthesis and application of magnetic iron oxide nanoparticles on the removal of Reactive Black 5: Reaction mechanism, temperature and pH effects', *J. Environ. Manage.*, vol. 224, pp. 235–242, Oct. 2018, doi: 10.1016/j.jenvman.2018.07.021.

[5] P. Mondal and M. K. Purkait, 'Green synthesized iron nanoparticles supported on pH responsive polymeric membrane for nitrobenzene reduction and fluoride rejection study: Optimization approach', *J. Clean. Prod.*, vol. 170, pp. 1111–1123, 2018, doi: 10.1016/j.jclepro.2017.09.222.

[6] G. Gnanaprakash, S. Mahadevan, T. Jayakumar, P. Kalyanasundaram, J. Philip, and B. Raj, 'Effect of initial pH and temperature of iron salt solutions on formation of magnetite nanoparticles', *Mater. Chem. Phys.*, vol. 103, no. 1, pp. 168–175, May 2007, doi: 10.1016/j.matchemphys.2007.02.011.

[7] F. Rehman, M. Sayed, J. A. Khan, and L. Ali, 'Degradation of Crystal Violet Dye by Fenton and Photo-Fenton Oxidation Processes', 2018.

[8] N. M. Mahmoodi, S. Keshavarzi, and M. Ghezelbash, 'Synthesis of nanoparticle and modelling of its photocatalytic dye degradation ability from colored wastewater', *J. Environ. Chem. Eng.*, vol. 5, no. 4, pp. 3684–3689, 2017, doi: 10.1016/j.jece.2017.07.010.

[9] R. Chavan *et al.*, 'Enhanced Photodegradation of Methylene Blue Using Reusable Cobalt Ferrite Nanocomposites', *Sci. Adv. Mater.*, vol. 16, no. 5, pp. 589–595, May 2024, doi: 10.1166/sam.2024.4689.

[10] A. Najafpoor *et al.*, 'Effect of magnetic nanoparticles and silver-loaded magnetic nanoparticles on advanced wastewater treatment and disinfection', *J. Mol. Liq.*, vol. 303, p. 112640, 2020, doi: 10.1016/j.molliq.2020.112640.

[11] P. Nicolás, M. Saleta, H. Troiani, R. Zysler, V. Lassalle, and M. L. Ferreira, 'Preparation of iron oxide

nanoparticles stabilized with biomolecules: Experimental and mechanistic issues', *Acta Biomater.*, vol. 9, no. 1, pp. 4754–4762, 2013, doi: 10.1016/j.actbio.2012.09.040.

[12] R. Chavan, R. Patil, and A. Chougale, 'Efficient Dye Removal Strategies : Exploring the Role of Biochar', *ChemSci Adv.*,vol. 1, no. 1, pp. 4–13, 2024.

[13] R. R. Chavan *et al.*, 'Catalytic Activity of CuO - bentonite Bead for the Removal of Methylene Blue by Fenton like Process', *ChemSci Adv.*,vol. 1, no. 2, pp. 96–104, 2024.

[14] C. C. Lin and J. M. Ho, 'Structural analysis and catalytic activity of Fe3O4 nanoparticles prepared by a facile co-precipitation method in a rotating packed bed', *Ceram. Int.*, vol. 40, no. 7 PART B, pp. 10275–10282, 2014, doi: 10.1016/j.ceramint.2014.02.119.

[15] A. Sirivat and N. Paradee, 'Facile synthesis of gelatin-coated Fe3O4 nanoparticle: Effect of pH in single-step co-precipitation for cancer drug loading', *Mater. Des.*, vol. 181, p. 107942, 2019, doi: 10.1016/j.matdes.2019.107942.

[16] M. A. A. Kerroum, A. Essyed, C. Iacovita, W. Baaziz, D. Ihiawakrim, and O. Mounkachi, 'The effect of basic pH on the elaboration of ZnFe 2 O 4 nanoparticles by co-precipitation method : Structural , magnetic and hyperthermia characterization', vol. 478, no. June 2018, pp. 239–246, 2019.

[17] K. Yang, H. Peng, Y. Wen, and N. Li, 'Re-examination of characteristic FTIR spectrum of secondary layer in bilayer oleic acid-coated Fe 3 O 4 nanoparticles', *Appl. Surf. Sci.*, vol. 256, no. 10, pp. 3093–3097, Mar. 2010, doi: 10.1016/j.apsusc.2009.11.079.

[18] A. Jafari, S. Farjami Shayesteh, M. Salouti, and K. Boustani, 'Effect of annealing temperature on magnetic phase transition in Fe3O4 nanoparticles', *J. Magn. Magn. Mater.*, vol. 379, pp. 305–312, Apr. 2015, doi: 10.1016/j.jmmm.2014.12.050.

[19] Z. Bilici, Z. Işık, Y. Aktaş, H. C. Yatmaz, and N. Dizge, 'Photocatalytic effect of zinc oxide and magnetite entrapped calcium alginate beads for azo dye and hexavalent chromium removal from solutions', *J. Water Process Eng.*, vol. 31, no. January, 2019, doi: 10.1016/j.jwpe.2019.100826.

[20] W. J. Jeyarani, T. Tenkyong, N. Bachan, D. A. Kumar, and J. M. Shyla, 'An investigation on the tuning effect of glucose-capping on the size and bandgap of CuO nanoparticles', *Adv. Powder Technol.*, vol. 27, no. 2, pp. 338–346, Mar. 2016, doi: 10.1016/j.apt.2016.01.006.

[21] Z. Zhang and J. Kong, 'Novel magnetic Fe3O4@C nanoparticles as adsorbents for removal of organic dyes from aqueous solution', *J. Hazard. Mater.*, vol. 193, pp. 325–329, 2011, doi: 10.1016/j.jhazmat.2011.07.033.

[22] Q. Inamur, M. Ahmad, S. Kumar, and M. Lohani, 'Effective photocatalytic degradation of rhodamine B dye by ZnO nanoparticles', vol. 91, pp. 170–174, 2013.

[23] C. C. Chen, W. C. Chen, M. R. Chiou, S. W. Chen, Y. Y. Chen, and H. J. Fan, 'Degradation of crystal violet by an FeGAC/H 2O 2 process', *J. Hazard. Mater.*, vol. 196, pp. 420–425, Nov. 2011, doi: 10.1016/j.jhazmat.2011.09.042.

[24] A. Jadhav *et al.*, 'Photocatalytic Degradation of Crystal Violet Dye Using Iron Oxide Nanoparticles', *J. Nanoelectron. Optoelectron.*, vol. 19, no. 3, pp. 272–277, Apr. 2024, doi: 10.1166/jno.2024.3571.

[25] N. Nadeem *et al.*, 'Degradation of reactive dye using heterogeneous photo-Fenton catalysts: ZnFe2O4 and GO-ZnFe2O4 composite', *Mater. Res. Express*, vol. 7, no. 1, 2020, doi: 10.1088/2053-1591/ab66ee.

[26] A. Tolba, M. Gar Alalm, M. Elsamadony, A. Mostafa, H. Afify, and D. D. Dionysiou, 'Modeling and optimization of heterogeneous Fenton-like and photo-Fenton processes using reusable Fe3O4-MWCNTs', *Process Saf. Environ. Prot.*, vol. 128, pp. 273–283, Aug. 2019, doi: 10.1016/j.psep.2019.06.011.

[27] A. Jadhav *et al.*, 'Photocatalytic Degradation of Crystal Violet Dye Using Iron Oxide Nanoparticles', *J. Nanoelectron. Optoelectron.*, vol. 19, no. 3, pp. 272–277, 2024, doi: 10.1166/jno.2024.3571.

[28] W. He *et al.*, 'Facile synthesis of Fe3O4@MIL-100(Fe) towards enhancing photo-Fenton like degradation of levofloxacin via a synergistic effect between Fe3O4 and MIL-100(Fe)', *Chem. Eng. J.*, vol. 409, Apr. 2021, doi: 10.1016/j.cej.2020.128274.

[29] X. Yang, W. Chen, J. Huang, Y. Zhou, Y. Zhu, and C. Li, 'Rapid degradation of methylene blue in a novel heterogeneous Fe3O4 @rGO@TiO2-catalyzed photo-Fenton system', *Sci. Rep.*, vol. 5, May 2015, doi: 10.1038/srep10632.

[30] F. Rehman *et al.*, 'Degradation of crystal violet dye by fenton and photo-fenton oxidation processes', *Zeitschrift fur Phys. Chemie*, vol. 232, no. 12, pp. 1771–1786, Dec. 2018, doi: 10.1515/zpch-2017-1099.

[31] R. R. Chavan *et al.*, 'Catalytic and kinetic studies of CuFe2O4 as a superior heterogeneous nanocatalyst for dye degradation and Cr(VI) reduction', *Clean Technol. Environ. Policy*, 2024, doi: 10.1007/s10098-023-02727-5.

[32] Y. She, 'Efficient Removal of Organic Pollutants with Magnetic Nanoscaled BiFeO 3 as a Reusable Heterogeneous Fenton-Like Catalyst', vol. 44, no. 5, pp. 1786–1791, 2010.

[33] P. K. Boruah, B. Sharma, I. Karbhal, M. V. Shelke, and M. R. Das, 'Ammonia-modified graphene sheets decorated with magnetic Fe3O4 nanoparticles for the photocatalytic and photo-Fenton degradation of phenolic compounds under sunlight irradiation', *J. Hazard. Mater.*, vol. 325, pp. 90–100, Mar. 2017, doi: 10.1016/j.jhazmat.2016.11.023.

